Dynamic light scattering study of internal motions of polymer coils in dilute solution

ARTICLE *in* MACROMOLECULES · DECEMBER 1991

Impact Factor: 5.8 · DOI: 10.1021/ma00026a005

Dynamic Light Scattering Study of Internal Motions of Polymer Coils in Dilute Solution

Benjamin Chu,* Zhulun Wang, and Jiqun Yu

Department of Chemistry, State University of New York, Stony Brook, New York 11794-3400

Received April 18, 1991; Revised Manuscript Received July 12, 1991

ABSTRACT: Internal motions of a high molecular weight (M_w = 8.12 × 10^6) polystyrene with a narrow distribution of $M_z/M_w \leq 1.04$ in benzene has been studied by dynamic light scattering. By means of a prism-cell light-scattering spectrometer, the translational diffusion of the center of mass of the polymer coil has been precisely determined at $KR_g \ll 1$ corresponding to using the self-beating technique at a scattering angle $\theta \leq 3°$. With the experimentally measured translational diffusion coefficient, a solid base for internal motion studies could be formulated. The first cumulant Ω obtained from the cumulants analysis of the measured intensity time correlation function approached K^3 dependence at $KR_g > 1$, indicating that the polymer chain dynamics could be described in terms of the non-free-draining model. Extraction of information on the internal motions was made by comparing the CONTIN output line-width distributions from the experimental data with those from the simulated data based on a theoretical model for polymer coils in the non-free-draining limit. By selecting appropriate KR_g ranges, the first two internal relaxation times could be obtained. At regimes of $1 \leq x \leq 3$ and $3 \leq x \leq 6$, where $x = (KR_g)^2$, the first internal relaxation time τ_1 (the longest one) and the second internal relaxation time τ_2 were determined, respectively. To our knowledge, for a flexible polymer coil in solution, τ_2 was determined experimentally for the first time. The experimental observations agreed very well with the theoretical predictions based on polymer chain dynamics with hydrodynamic interactions.

I. Introduction

The dynamics of polymer chains in dilute solution is one of the fundamental problems in polymer physics. The theory of dynamic properties of flexible polymer chains has been developed by Rouse[1] and Zimm,[2] i.e., the well-known Rouse–Zimm (RZ) model. Experimental advances in investigating the dynamics of flexible polymers in solution have been made possible partially by the developments of better dynamic light scattering instrumentation and of more sophisticated methods of data analysis.[3-5] The RZ model has been applied to dynamic light scattering studies by Pecora,[6] de Gennes,[7] and DuBois-Violette[8] who established forms for the dynamic structure factor $S(K,t)$. In the region $KR_g \ll 1$ with K (= $(4\pi n/\lambda_0) \sin(\theta/2)$) and R_g being, respectively, the scattering vector and the radius of gyration of the polymer chains, the contribution to $S(K,t)$ is mainly from the translational diffusion of the center of mass of the polymer chains. Thus, $S(K,t)$ at $KR_g \ll 1$ and for monodisperse polymer coils has a single exponential form. In the intermediate KR_g range with $KR_g \geq 1$ and even for monodisperse polymer chains, $S(K,t)$ becomes multiexponential due to significant contributions from various internal motions. Investigation of intramolecular internal motions in the polymer chain having internal degrees of freedom is of particular interest because such studies may permit us to obtain information on the flexibility parameter for flexible and semiflexible polymers. However, study of internal motions in dilute polymer solutions has remained a difficult experimental problem especially when a proper interpretation of $S(K,t)$ needs an appropriate theoretical model.[9]

Akcasu et al.[10] have developed a method for the interpretation of dynamic light scattering data over the entire accessible K range in terms of the first cumulant $\Omega(K)$ of $S(K,t)$ which is the initial slope of $S(K,t)$ and can be determined by the cumulants analysis[11] of $S(K,t)$. This practical approach is quite useful in testing the dynamic models with or without hydrodynamic interactions.[12] It was found that $\Omega(K)$ had a K^2 dependence for $KR_g \ll 1$ and a K^3 dependence for $KR_g \gg 1$ in polystyrene dilute solutions.[12]

Investigation of internal motions for flexible coils[12-17] and wormlike chains[18-20] have been reported recently. However, the determination of local internal motions is often difficult because very high molecular weight polymers with narrow molecular weight distributions should be used in order to reach $KR_g \gg 1$. Yet, measurements at small scattering angles should be made in order to obtain a reference state in terms of pure translational motions of the center of mass of polymer chains. Separation of internal motions and translational motions can be carried out by using various data analysis methods, e.g., the CONTIN method,[21] the double exponential or multiexponential fitting method,[22] the histogram method,[23] and the discrete inversion method.[17] The slowest mode is usually attributed to the translational motion while faster ones are assigned to internal relaxation modes which could be coupled to the translational motions.

The Laplace inversion problem can only be accepted with caution in the case of two closely spaced bimodal distributions.[24] For example, with poly(α-methylstyrene) in toluene, which is similar to the present system, a clear separation into two components was obtained only for $KR_g > 2$ by the discrete inversion method.[17] The CONTIN method, using a regularization technique to seek smooth solutions, is appropriate for correlation profile analysis without an a priori assumption on the form of the distribution. But as pointed out by Pecora,[18] data analysis involving internal motions often requires the resolution limit of CONTIN because the dominating term of the intensity–intensity time correlation function is the translational motion term. With the addition of internal motions, the time correlation function then exhibits multimodal characteristics which often become difficult to resolve due to the low resolution of the Laplace inversion (see eq 2 in the following section). Furthermore, we used CONTIN instead of MEM[31] or other comparable algorithms

* Author to whom all reprint requests should be addressed.

0024-9297/91/2224-6832$02.50/0

because CONTIN is more widely used and similar results would have been obtained, independent of the method of data analysis. Thus, experimental determinations on the internal modes of polymer chains have been difficult to achieve.

We present an investigation of internal motions from the measured intensity time correlation function by dynamic light scattering. In comparison with the theoretical model, we demonstrated that, in addition to the longest internal relaxation time τ_1, the second internal relaxation time τ_2 could also be determined under appropriate conditions. The experimental determination of τ_2 represents, to our knowledge, the first such measurement for a polymer coil with hydrodynamic interactions. In order to achieve this feat, we need a monodisperse polymer with an appropriate size which will permit us to measure the pure translational diffusion at small but accessible scattering angles and yet large enough in size for studies of internal motions at higher scattering angles. As dynamic light scattering has a limited K range, the small KR_g value implies that we need to make the linewidth measurements at small scattering angles such as those available by the specially designed prism-cell light-scattering spectrometer[25] which permits self-beating linewidth measurements at scattering angles of the order of a few degrees. Finally, in order to resolve the different relaxation times, it is necessary to obtain precise intensity time correlation function data over an appropriate range of scattering angles which are governed by polymer size, polymer dynamics, and light wavelength. With a combination of the above requirements and conditions, we can then proceed to determine τ_2.

Dilute solutions of a monodisperse 8×10^6 Da molecular weight polystyrene in benzene were used. By taking advantage of the prism-cell laser light-scattering spectrometer, very small scattering angles of the order of $\sim 2°$ would be reached in the present experiments. Thus the pure translational motion term in $S(K,t)$ could be determined precisely. By applying the CONTIN method to the analysis of $S(K,t)$ at $KR_g > 1$, internal motion information could then be extracted. The simulated correlation function based on a theoretical model for flexible polymer chain dynamics with hydrodynamic interactions[2,26] was also analyzed by the CONTIN method. At least the first two longest internal relaxation times, τ_1 and τ_2, could be evaluated by working at proper KR_g ranges. The values of the experimentally determined internal relaxation times τ_1 and τ_2 were in good agreement with the theoretical predictions based on the non-free-draining model.[2]

II. Experimental Method

Correlation Function Measurement and Data Analysis. The measured self-beating photocount time correlation function from photon correlation spectroscopy (PCS) has the form

$$G^{(2)}(t) = A(1 + \beta|g^{(1)}(t)|^2) \tag{1}$$

where A is the background, β is a spatial coherent factor, and $g^{(1)}(K,t)[\sim S(K,t)]$ is the normalized first-order electric field correlation function. At $KR_g \ll 1$, or for structureless particles without internal motions, the normalized characteristic line-width distribution $G(\Gamma)$ can be evaluated by performing the Laplace inversion

$$|g^{(1)}(t)| = \int_0^\infty G(\Gamma)e^{-\Gamma t}\,d\Gamma \tag{2}$$

with an average characteristic linewidth $\bar{\Gamma}$ ($= \int \Gamma G(\Gamma)\,d\Gamma$) $= \bar{D}K^2$ and $\bar{D}$ being the average translational diffusion coefficient. From experimental data, we can compute the peaks in $G(\Gamma)$ in terms of continuous or discrete line widths $\bar{\Gamma}_i$. In practice, most peaks have very narrow distributions. So we use $\bar{D} = D$ and $\bar{\Gamma}_i = \Gamma_i$ interchangeably. At $KR_g > 1$, the contribution of internal motions to the scattering function becomes appreciable.

The dynamic structure factor for a flexible chain has a complex form of

$$S(K,t) = e^{-DK^2t}\sum_{n=1}^{\infty} S_n(K,t) \tag{3}$$

where $S_n(K,t)e^{-DK^2t}$ are the dynamic light scattering (DLS) relaxation modes whose forms have been predicted by Pecora et al.[18] for the free-draining model of a flexible coil. Concerning the effect of hydrodynamic interactions, Perico et al.[26] calculated the spectral distribution of light scattering from flexible polymer coils in solution on the basis of the bead and spring model in the non-free-draining limit. They found that with hydrodynamic interactions the effect of internal motions became more pronounced when compared with the free-draining case. At $KR_g \geq 1$, $S(K,t)$ depends only on five decay rates, coming from a pure translational term and four principal intramolecular terms. Equation 3 can thus be approximately expressed as

$$S(K,t) = S_1(K)\exp(-DK^2t) + S_2(K)\exp[-(DK^2 + 2/\tau_1)t] + S_3(K)\exp[-(DK^2 + 1/\tau_2)t] + S_4(K)\exp[-(DK^2 + 4/\tau_1)t] + S_5(K)\exp[-(DK^2 + 2/\tau_2)t] + \ldots \tag{4}$$

where the intensity factor $S_n(K)$ is KR_g dependent and τ_n is the relaxation time of the nth internal mode which is twice the Zimm normal mode relaxation time.[2] It should be noted that (a) $S_n(K,t)e^{-DK^2t}$ are referred to as the DLS relaxation modes, (b) τ_n is the relaxation time of the nth internal mode, (c) $S_n(K)$ is the intensity factor of the nth DLS relaxation mode, and (d) each DLS relaxation mode has a characteristic line width (or decay rate). For example, for the 4th DLS relaxation mode, the intensity factor is $S_4(K)$, the characteristic decay rate is $DK^2 + 4/\tau_1$, and the relaxation time comes from the first internal mode τ_1. In particular, although there are five decay rates, there are only *two* internal modes in addition to the translational motions. In contrast to the above definitions, the experimental data yield only an estimate of $G(\Gamma)$ which could contain a number of "peaks". Each experimental peak may contain a single DLS relaxation mode, such as $S_1(K)e^{-DK^2t}$ for the pure translational motions or it may contain unresolved modes which are coupled together into a broader unresolved peak. All the decay rates in the DLS relaxation modes contain the DK^2 term, which makes the separation of internal modes more difficult especially when DK^2 is not known.

Perico et al.[26] have also calculated the numeric values of intensity factors of the above five decay rates, i.e., $S_n(K)$ (n = 1, 2, 3, 4, and 5), at values of x from 1 to 10, where $x = (KR_g)^2$, in the non-free-draining limit. Thus the theoretical dynamic structure factor $S(K,t)$ is available in the literature. A comparison of the output of the line-width (or decay rate) distribution between the simulated data and the experimental data is made in order to provide a basis for extracting the internal modes correctly.

Instrumentation. The prism-cell laser light-scattering spectrometer has been described elsewhere.[25] The spectrometer used a unique prism light-scattering cell capable of making small-angle self-beating dynamic light-scattering measurements down to a scattering angle of about 2° and is able to achieve an optical coherence factor β of ~ 0.9 routinely. An argon ion laser operated at a wavelength of 488 nm was used as a light source. A conventional laser light-scattering spectrometer which has been described in ref 27 was also used for making measurements at large scattering angles. The argon ion laser in the conventional laser light-scattering spectrometer was operated at a different wavelength of 514.5 nm. The experimental results could be verified more convincingly by using two different wavelengths because the τ values are invariant. A Brookhaven BI2030 autocorrelator with 64 channels was used to measure the intensity time correlation function $G^{(2)}(t)$. The measurements were performed at 25 ± 0.05 °C. Both CONTIN[21] and cumulants[11] methods were used to analyze the data.

Materials. A narrow molecular weight distribution polystyrene (PS) sample purchased from Polymer Laboratories with $M_p = 8.00 \times 10^6$ g/mol and $M_w/M_n \leq 1.10$ was used in the present

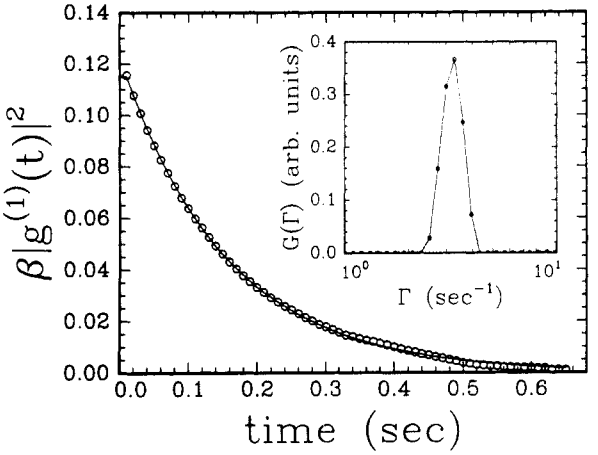

Figure 1. A typical measured net intensity time correlation function for PS in benzene at $KR_g \ll 1$. The measurement was performed at $\theta = 2.88°$ ($KR_g = 0.18$) and 25 °C with a sample concentration of 7.55×10^{-5} g/mL. The line denotes the fitting result from the CONTIN analysis. A unimodel characteristic line-width distribution as shown in the inset was obtained from CONTIN. The average line width $\bar{\Gamma} = 3.25$ s^{-1} and the variance Var ($= \mu_2/\bar{\Gamma}^2$) = 0.01 with $\mu_2 = \int(\Gamma-\bar{\Gamma})^2 G(\Gamma)\, d\Gamma$.

study. Our independent light-scattering experiments showed $M_w = 8.12 \times 10^6$ g/mol which was based on a comparison of our measured diffusion coefficient at infinite dilution with the expression[28]

$$D_0 = [(2.18 \pm 0.32) \times 10^{-4}]M^{-(0.55\pm0.02)}\ (\text{cm}^2/\text{s}) \qquad (5)$$

$M_z/M_w \leq 1.04$ was determined from the measured variance of the intensity–intensity time correlation function. Spectrograde benzene was used as a solvent without further purification. The overlap concentration C^*, estimated according to the following equation:

$$C^* = M/(N_A R_g^3) \qquad (6)$$

with N_A being Avogadro's number, was about 2.1×10^{-3} g/mL for the present PS/benzene system. Two solutions at concentrations of 9.44×10^{-6} and 7.55×10^{-5} g/mL, respectively, were prepared. Both concentrations were much smaller than C^* in order to ensure an absence of appreciable intermolecular interactions. The PS sample was first dissolved in dust-free benzene solvent for at least a one-week time period. The polymer solution was then centrifuged at 1000g for ca. 8 h before light-scattering measurements. Clarification of solution was particularly important for light-scattering measurements at small scattering angles and for obtaining high-precision data at large scattering angles for the purpose of internal motion studies.

III. Results and Discussions

Pure Translational Mode ($KR_g \ll 1$). With the 8 million molecular weight PS in benzene, $R_g \simeq 185$ nm[28] which can be translated to a scattering angle θ of about 16° for $KR_g = 1$ with $\lambda_0 = 488$ nm, and the refractive index of the solvent $n \simeq 1.5$. $\theta \leq 16°$ is not easily accessible using a normal light-scattering spectrometer. With our prism-cell light-scattering spectrometer, $G^{(2)}(t)$ could be measured at $KR_g \ll 1$. Figure 1 shows a typical measured net intensity time correlation function and the CONTIN analysis results. A unimodal characteristic line-width distribution with a very small variance ($\mu_2/\bar{\Gamma}^2$) was obtained by the CONTIN analysis, indicating that $S(K,t)$ contained only the pure translational diffusion contribution. A very small value of ≤0.01 for the variance confirmed that the PS sample was very monodisperse. In the vicinity of $KR_g = 1$, e.g., $KR_g = 0.95$ or $\theta = 15.24°$, the CONTIN analysis already yielded a bimodal line-width distribution but the area ratio of the second peak in $G(\Gamma)$ was only about 1.3%. The translational diffusion coefficient D (= $\bar{\Gamma}/K^2$) usually has a concentration dependence as follows:

$$D = D_0(1 + k_D C) \qquad (7)$$

where D_0 is the D value extrapolated to infinite dilution and k_D is a constant. The deviation of D measured at a certain concentration from D_0 could be estimated on the basis of the reported value of k_D for the PS/benzene system.[16] With the present two concentrations, the measured D value should be within 4% of D_0 on the basis of the k_D value reported in ref 16. Table I lists the results from the CONTIN analysis. The translational diffusion coefficient was independent of scattering angle and concentration. The average diffusion coefficient $\bar{D}$ was $3.45 \times 10^{-8}(\pm 3\%)$ cm^2/s with a variance of only ≤0.01.

Table I
CONTIN Analysis of PCS Data of Dilute Solutions of Polystyrene in Benzene at $KR_g < 1$

angle θ	KR_g	N^a	$\bar{\Gamma}_N$, s^{-1}	Var_N	$\bar{\Gamma}_N/K^2$, cm^2/s	A_N, %^{b}
2.88	0.18	1	3.25	0.01	3.40×10^{-8}	100
4.87	0.31	1	9.92	0.004	3.63×10^{-8}	100
6.19^c	0.39	1	14.8	0.009	3.35×10^{-8}	100
10.12	0.63	1	39.7	0.004	3.37×10^{-8}	100
15.24	0.95	1	92.8	0.02	3.48×10^{-8}	98.7
		2	1.21×10^3	0.003	4.54×10^{-7}	1.3

^{a} N denotes peak number in $G(\Gamma)$. 1 means the peak with the lowest frequency. If 2 is not there, 1 also denotes that $G(\Gamma)$ is unimodal. ^{b} A_N (%) is the area ratio of peak i in the $G(\Gamma)$ distribution curve. ^{c} The data was obtained from a sample with a concentration of 9.44×10^{-6} g/mL at a scattering angle $\theta = 6.19°$. Measurements at other scattering angles were obtained from a sample with a concentration of 7.55×10^{-5} g/mL.

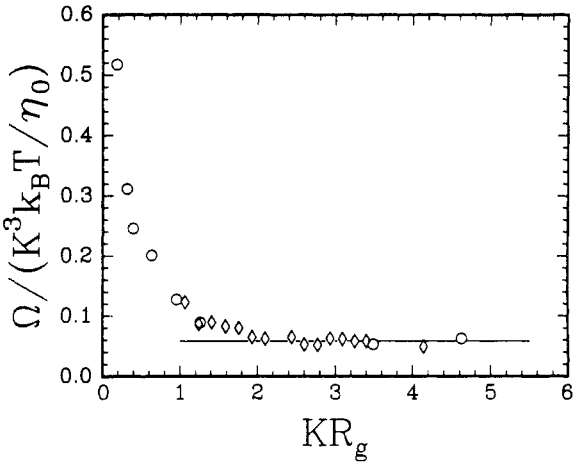

Figure 2. Plot of the reduced first cumulant $\Omega/(K^3k_BT/\eta_0)$ versus KR_g for dilute solutions of PS in benzene. η_0 is the solvent viscosity. The first cumulant Ω was obtained from the cumulants analysis. Circles represent the data points measured by the prism-cell light-scattering spectrometer and diamonds, by the normal light-scattering spectrometer. The reduced first cumulants approached a constant value with increasing KR_g values. The line denotes the plateau value of the reduced first cumulant (0.059 ± 0.005) at $KR_g \geq 2$.

Reduced First Cumulant. At $KR_g > 1$, the time correlation function could reveal contributions due to internal motions. On the basis of the cumulants approach, the first cumulants Ω[10] of $S(K,t)$ were calculated by using the third order fit of the cumulants expansion.[11] Figure 2 shows the variation of the reduced first cumulant $\Omega(K)/(K^3k_BT/\eta_0)$ as a function of KR_g, where k_B is the Boltzmann constant, T is the absolute temperature, and η_0 is the solvent viscosity. With increasing KR_g values, the reduced first cumulant decreased and approached a constant value at $KR_g \gtrsim 2$. The first cumulant which could be scaled with K^3 instead of K^4 was consistent with the

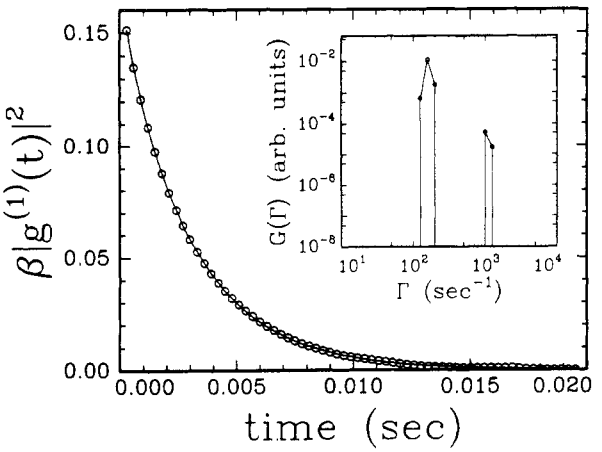

Figure 3. A typical measured net intensity time correlation function for PS in benzene at $KR_g = 1.24$ or scattering angle $\theta = 21°$, $T = 25$ °C, and $C = 7.55 \times 10^{-5}$ g/mL. The line denotes the fitting result from the CONTIN analysis. A bimodal characteristic linewidth distribution was obtained from CONTIN as shown in the inset with average line-widths $\bar{\Gamma}_1 = 168$ s^{-1}, $\bar{\Gamma}_2 = 1.12 \times 10^3$ s^{-1}, variance $Var_1 = 0.02$ and $Var_2 = 0.01$.

non-free-draining bead–spring theoretical model for flexible polymer chains.[8] The K^3 dependence of the first cumulant had also been reported for high molecular weight polystyrene solutions.[12,16] However, the constant value of the reduced first cumulent (0.059 ± 0.005) was lower than the theoretical value (of 0.071 for non-free-draining flexible coils with a preaveraged Oseen tensor and 0.079 without a preaveraged Oseen tensor).[12] Our plateau value, after correction for the finite concentration dependence as denoted by eq 7 where the experimental D/D_0 ratio at the concentration we used is 1.04, has a value of 0.059/1.04 = 0.057 and is in excellent agreement with the experimental value of 0.057 reported by Nemoto et al.[16]

Extraction of Internal Modes. At $KR_g \geq 1$, the application of CONTIN to the measured time correlation function yielded at least a bimodal line-width distribution as shown in Figure 3. The first peak in the line-width distribution which is also the slowest one is generally attributed to the translational diffusion of the center of mass of polymer chain only. However, this kind of consideration is based on the assumption that the characteristic line widths due to the translational diffusion and internal motions are separated far enough from one another and that there are *no* interactions between the translational and internal modes. Unfortunately, the assumption is not always true. Table II lists the CONTIN analysis results at $KR_g > 1$. The increasing values of the variance (>0.01) of the first peak clearly indicated otherwise. From the $\theta = 15.24°$ ($\sim KR_g = 0.95$) measurement as listed in Table I, one may note that although the D ($=\Gamma_1/K^2$) of 3.48×10^{-8} cm^2/s is within the error limits of the average D value for the pure translational motion, the variance (~ 0.02) has already been slightly larger. At higher scattering angles and at $KR_g > 1$, the D values become larger by $\sim 8\%$ and are constant over a KR_g range of $1 \leq KR_g \leq 1.8$. Figure 4 shows the K dependence of Γ/K^2, where Γ is the total average line width in a unimodal distribution or the average line width from the first peak in a bimodal (or multimodal) distribution. When $KR_g > 1$, the values of Γ/K^2 from the first peak deviated from the constant value obtained at $KR_g < 1$, indicating that even the first peak in the multimodal distribution as determined by CONTIN does not involve only pure translational diffusion but must have already coupled with some internal motion contributions due mainly to the low resolution of Laplace inversion by means of eq 2. In practice, it implies that precise translational motions should be measured only at $KR_g < 1$, and evaluation of internal motions could not be made by simply attributing the second (and the third) peak to the first (and the second) mode of internal motions.

In the non-free-draining limit, the internal relaxation times can be estimated according to the Rouse–Zimm model:[2]

$$\tau_n = \frac{M\eta_0[\eta]}{0.293RT\lambda_n'} \tag{8}$$

where λ_n's are given in ref 29 in which $\lambda_1' = 4.04$, $\lambda_2' = 12.79$ and $\lambda_3' = 24.2$, $[\eta]$ is the intrinsic viscosity, M is the molecular weight, and R is the gas constant. For polystyrene in benzene, the intrinsic viscosity can be obtained from an empirical relation:[30]

$$[\eta] = 7.8 \times 10^{-3} M_w^{0.75} \tag{9}$$

with $[\eta]$ and M_w expressed in units of milliliter per gram and gram per mole, respectively. The theoretical values of τ_1, τ_2, and τ_3 were 2.02×10^{-3}, 6.37×10^{-4}, and 3.38×10^{-4} s, respectively.

For flexible polymer coils, Perico et al.[26] pointed out that the intramolecular motion contributions increased with increasing KR_g value. They also predicted that at $1 \leq x \leq 3$, only the first internal mode τ_1 gives a significant contribution to $S(K,t)$. While at $3 \leq x \leq 6$ both the first and second mode, i.e., τ_1 and τ_2, have appreciable contributions to $S(K,t)$, resulting in five line widths in the spectral distribution.

The experimental observations were very interesting. At $1 \leq x \leq 3$, basically bimodal line-width distributions were obtained from CONTIN (see Table II) with the average decay rate of the first peak deviating from DK^2 slightly. From the average line width of the second peak (the faster one) which contained the information on intramolecular motions, the internal relaxation time ($\tau = 2/(\bar{\Gamma}_2 - DK^2)$) could be deduced, i.e., $\tau = 1.90 \times 10^{-3}$, 2.07×10^{-3}, 2.07×10^{-3}, and 1.81×10^{-3} s for $KR_g = 1.06$, 1.24, 1.41, and 1.59, respectively. The obtained internal relaxation times were in very good agreement with the theoretically predicted τ_1 value of 2.02×10^{-3} s.

At $3 \leq x \leq 6$, most of the line-width distributions were still bimodal. Although multimodal distributions were observed at some KR_g values, the contributions of the third peak (e.g., $\theta = 30°$ and 60°) were very small and were of the order of experimental noise. The obtained internal relaxation times from the second peak were, respectively, 6.39×10^{-4}, 6.90×10^{-4}, 6.71×10^{-4} and 6.62×10^{-4} s for $KR_g = 1.93$, 2.10, 2.44, and 2.60. These measured relaxation times were in coincidence with the theoretical predicted relaxation time of the *second* internal mode τ_2 of 6.37×10^{-4} s, instead of with the first internal mode τ_1 which was expected to remain a dominant term at this KR_g regime. However, both the average line width and the variance of the first peak increased, i.e., Γ_1/K^2 increased from 3.45×10^{-8} cm^2/s to $\sim 4.4 \times 10^{-8}$ cm^2/s and Var_1 from 0.01 to ~ 0.05, indicating that not only the pure translational motion but also some internal modes had some contributions to the first peak.

Furthermore, the relaxation times deduced from the second peak at $6 < x < 10$ were reasonably close to the theoretical value of 3.38×10^{-4} s for the third internal relaxation time τ_3. At even higher values of KR_g, e.g., $KR_g = 4.14$ and 4.62, very broad bimodal line-width distributions with $Var_1 \sim 0.45$ were observed, suggesting that at this KR_g regime, the average characteristic line widths

Table II
CONTIN Analysis of PCS Data of Dilute Solutions of Polystyrene in Benzene at $KR_g \geq 1$

θ	KR_g	x	N	$\bar{\Gamma}_N$, s^{-1}	Var_N	A_N, %	$\bar{\Gamma}_1/K^2$, cm^2/s	$\tau = 2/(\bar{\Gamma}_2 - DK^2)$,[a] s
18	1.06	1.12	1	124	0.02	96.9	3.75×10^{-8}	
			2	1.16×10^3	0.008	3.1		1.90×10^{-3}
21	1.24	1.54	1	168	0.02	96.4	3.74×10^{-8}	
			2	1.12×10^3	0.01	3.6		2.07×10^{-3}
24	1.41	1.99	1	220	0.04	95.3	3.76×10^{-8}	
			2	1.17×10^3	0.000	4.7		2.07×10^{-3}
27	1.59	2.53	1	276	0.03	93.6	3.74×10^{-8}	
			2	1.36×10^3	0.006	5.4		1.81×10^{-3}
30	1.76	3.10	1	343	0.04	90.4	3.79×10^{-8}	
			2	1.41×10^3	0.02	8.2		1.81×10^{-3}
			3	1.61×10^4	0.000	1.4		
33	1.93	3.72	1	478	0.09	95.8	4.39×10^{-8}	
			2	3.51×10^3	0.014	4.2		6.39×10^{-4}
36	2.10	4.41	1	568	0.05	94.1	4.40×10^{-8}	
			2	3.34×10^3	0.02	5.9		6.90×10^{-4}
42	2.44	5.95	1	728	0.03	89.6	4.18×10^{-8}	
			2	3.58×10^3	0.05	10.4		6.71×10^{-4}
45	2.60	6.76	1	957	0.21	91.9	4.83×10^{-8}	
			2	3.70×10^3	0.02	7.0		6.62×10^{-4}
			3	1.17×10^4	0.000	1.1		
48	2.77	7.67	1	1.12×10^3	0.14	12.6	5.00×10^{-8}	
			2	7.10×10^4	0.02	0.9		3.16×10^{-4}
			3	4.54×10^5	0.24	86.5		
51	2.93	8.58	1	1.22×10^3	0.05	90.3	4.86×10^{-8}	
			2	7.56×10^3	0.02	9.7		2.99×10^{-4}
54	3.09	9.55	1	1.36×10^3	0.07	87.9	4.87×10^{-8}	
			2	6.66×10^3	0.01	12.1		3.51×10^{-4}
57	3.25	10.6	1	1.54×10^3	0.06	11.0	5.00×10^{-8}	
			2	6.91×10^3	0.01	1.7		3.42×10^{-4}
			3	4.72×10^5	0.22	82.0		
60	3.40	11.6	1	1.77×10^3	0.10	3.6	5.24×10^{-8}	
			2	7.38×10^3	0.04	0.6		3.22×10^{-4}
			3	3.36×10^4	0.000	0.07		
			4	3.21×10^6	0.55	95.73		
75	4.14	17.1	1	4.23×10^3	0.44	0.6	8.44×10^{-8}	
			2	3.04×10^7	0.69	99.4		
80[b]	4.62	21.3	1	5.39×10^3	0.45	0.03	8.64×10^{-8}	
			2	4.72×10^7	0.66	99.97		

[a] Based on the assumption that $g^{(1)}(t) \approx S_1(K) \exp(-\bar{\Gamma}_1 t) + S_i(K) \exp(-\bar{\Gamma}_i t)$, where $\bar{\Gamma} = DK^2 + 2/\tau_i$, and the nature of τ_i is yet to be identified. Furthermore, the bimodal distribution was obtained experimentally without an a priori assumption that $G(\Gamma)$ should be bimodal. [b] The data at a scattering angle of 80° was from the prism-cell light-scattering spectrometer.

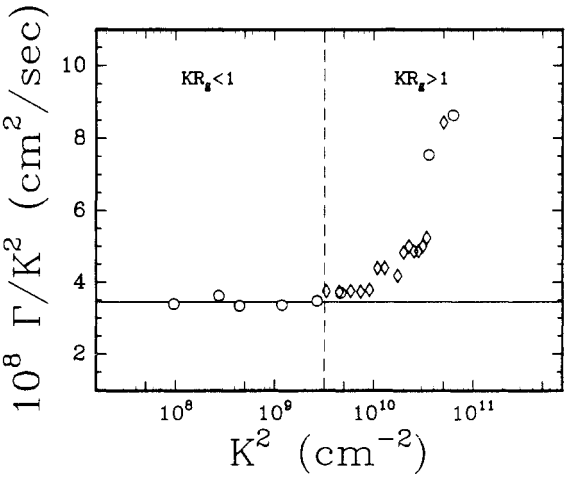

Figure 4. Plot of Γ/K^2 versus K^2 for dilute solutions of PS in benzene. At $KR_g \ll 1$, the value of Γ was the average characteristic line width for the unimodal distributions. At $KR_g \geq 1$, the values of Γ were the average characteristic line width of the first or the slowest peak in the bimodal or multimodal distributions. The line denotes an average value of Γ/K^2 ($= 3.45 \times 10^{-8}$ cm^2/s ($\pm 3\%$)) at $KR_g \ll 1$. Vertical dashed line denotes $KR_g = 1$. Circles denote measurements from the prism-cell light-scattering spectrometer. Diamonds denote measurements using a conventional light-scattering spectrometer.

were composites involving a more complex contribution of internal motions to the dynamic structure factor $S(K,t)$.

According to the theoretical work of Perico et al.,[26] the five decay rates of one translational term and four principal internal components, i.e., DK^2, $DK^2 + 2/\tau_1$, $DK^2 + 1/\tau_2$, $DK^2 + 4/\tau_1$, and $DK^2 + 2/\tau_2$, gave the major contributions to $S(K,t)$ at $KR_g \geq 1$. At $x = 3$, the four principal internal terms accounted for 90% of the total intramolecular contribution. At $x = 6$, the residual intramolecular intensity increased to about 20%.[26] Thus, at larger KR_g values, i.e., at $x > 6$, the evaluation of the internal modes becomes difficult because higher internal relaxation times like τ_3 and τ_4 have nonnegligible contributions to $S(K,t)$.

By using the experimentally measured pure translational term DK^2 and the calculated theoretical internal relaxation times τ_1 and τ_2, the above five decay rates were calculated (see Table III). It was noted that the four principal internal components resulting from the intramolecular motions were closely spaced. With increasing KR_g values, the separation in the decay rates between the pure translational term and the intramolecular terms decreased as shown in Figure 5, where the ratio of the decay rates from the intramolecular terms to the pure translational term versus KR_g was plotted. Concerning the resolution of the CONTIN analysis method, CONTIN may not be able to separate all terms in $S(K,t)$ even with high precision data. At $x > 3$, the first internal motion term was located closely to the pure translational term. Thus, despite its larger intensity factor, CONTIN might not be able to distinguish it from the translational term.

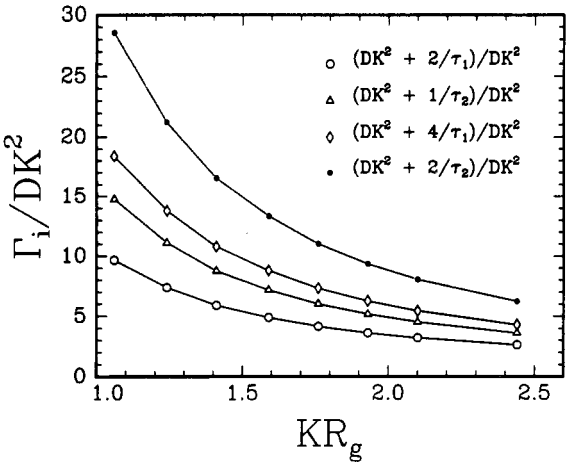

Figure 5. Plots of the ratios of the decay rates of the four principal intramolecular terms to that of the translational term DK^2 versus KR_g for the present PS/benzene system.

Table III
Calculated Decay Rates[a] of Five Principal DLS Relaxation Modes in $S(K,t)$ of Dilute Solutions of Polystyrene in Benzene

angle θ	KR_g	Γ_1, s^{-1}	Γ_2, s^{-1}	Γ_3, s^{-1}	Γ_4, s^{-1}	Γ_5, s^{-1}
18	1.06	114	1104	1684	2094	3254
21	1.24	155	1145	1725	2135	3295
24	1.41	202	1192	1772	2182	3342
27	1.59	254	1244	1824	2234	3394
30	1.76	313	1303	1883	2293	3453
33	1.93	376	1366	1946	2356	3516
36	2.10	445	1435	2015	2425	3585
42	2.44	600	1590	2170	2580	3740

[a] The five decay rates are $\Gamma_1 = DK^2$, $\Gamma_2 = DK^2 + 2/\tau_1$, $\Gamma_3 = DK^2 + 1/\tau_2$, $\Gamma_4 = DK^2 + 4/\tau_1$, and $\tau_5 = DK^2 + 2/\tau_2$, respectively, with DK^2 being measured from the experiment at $KR_g \ll 1$ and τ_1 and τ_2 being calculated from the Rouse–Zimm model in the non-free-draining limit.

Table IV
Characteristics of Line-Width Distributions from the CONTIN Analysis of Simulated Correlation Functions

	simulation without noise				simulation with added noise[a]			
x	N	$\bar{\Gamma}_N$, s^{-1}	Var_N	A_N, %	N	$\bar{\Gamma}_N$, s^{-1}	Var_N	A_N, %
1.54	1	156	0.008	95.4	1	161	0.03	97.8
	2	1.37×10^3	0.006	4.6	2	1.35×10^3	0.001	2.2
3.72	1	382	0.007	79.9	1	493	0.16	94.5
	2	1.55×10^3	0.004	18.5	2	3.16×10^3	0.02	5.5
	3	3.88×10^3	0.005	1.6				

[a] The random noise was added to the simulated noise-free correlation function data d_i^2, i.e., the noisy correlation data d_i^2 (with noise) $= d_i^2 + \mathrm{error}[1 + d_i^2]^{1/2}$, where error $= \mathrm{RN}/B^{1/2}$ was a normal deviate with zero mean and deviation $1/B^{1/2}$ with RN being random number. Here the added error $\leq 1\%$.

In order to compare the experimental observations to the theoretical predications, simulated correlation functions were generated according to the theoretical work by Perico et al.,[26] and then analyzed by CONTIN. The characteristics of two representative line-width distributions yielded by the CONTIN analysis of the simulated data in the two KR_g regimes of $1 \leq x \leq 3$ and $3 \leq x \leq 6$ are listed in Table IV. Figure 6 displays the line-width distributions from CONTIN of the measured correlation function (circle–solid line) and those from the simulated correlation functions with (diamond–dash–dot line) and without noise (triangle–dash line) at $x = 1.54$ ($KR_g = 1.24$). Bimodal line-width distributions were obtained from CONTIN for both the measured and the simulated data even without noise. On closer examination of the values of the decay rates (see Tables III and IV), the two peaks in the bimodal

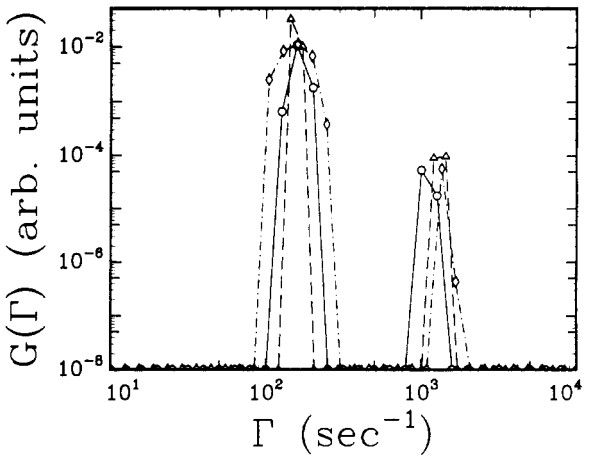

Figure 6. Plots of line-width distributions from the CONTIN analysis at $KR_g = 1.24$. The circle–solid line was from the measured PCS data. The triangle–dash line was from the simulated correlation function without noise. The diamond–dash–dot line was from the simulated correlation function with added noise (with error $\leq 1\%$). The experimental results agreed with the simulation results very well.

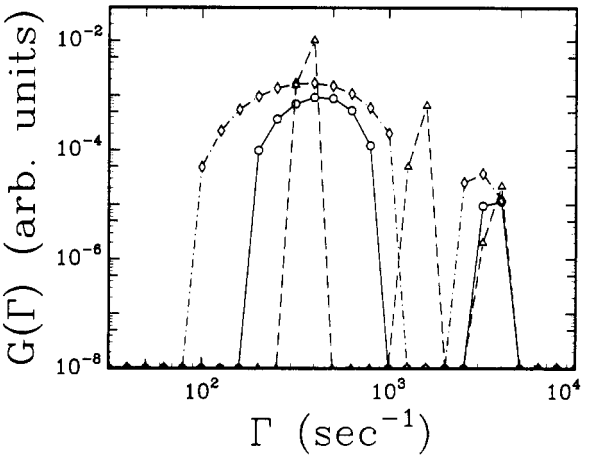

Figure 7. Plots of line-width distributions from the CONTIN analysis at $KR_g = 1.93$. The circle–solid line was from the measured PCS data. The triangle–dash line was from the simulated correlation function without noise. The diamond–dash–dot line was obtained from the simulated correlation function with added noise (with error $\leq 1\%$). Only a bimodal line-width distribution was yielded from the noisy simulated correlation function with the second peak corresponding to the intramolecular term of $DK^2 + 2/\tau_2$. This result was in agreement with the experimental observation.

distribution could be attributed to the translational term and the first principal internal term with a decay rate of $DK^2 + 2/\tau_1$. Therefore, at $1 \leq x \leq 3$, the first internal relaxation time could be determined without interference from the higher order internal motion terms since the intensity factor related to the $DK^2 + 2/\tau_1$ term dominates the whole intramolecular motions. At $x \geq 3$, the higher order internal motion terms begin to play a more important role in $S(K,t)$. At $3 \leq x \leq 6$, a comparison of the line-width distribution from CONTIN of the measured data (circle–solid line) with those of the noise-free (triangle–dash line) and noisy (diamond–dash–dot line) simulated correlation functions at $x = 3.72$ ($KR_g = 1.93$) is shown in Figure 7. With noise-free simulated data, the line-width distribution as listed in Table IV revealed a trimodal distribution with the three peaks being identified as the translational term DK^2, the first internal term ($DK^2 + 2/\tau_1$) and the forth internal term ($DK^2 + 2/\tau_2$), respectively (see Tables IV and III). But with the noisy simulated data, the line-width distribution became bimodal as we

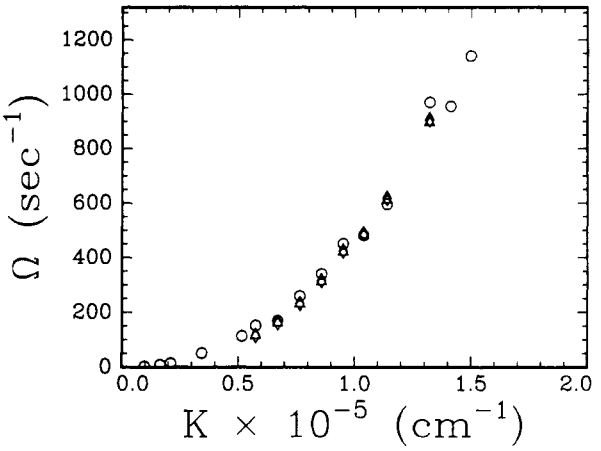

Figure 8. Plots of Ω versus K. Circles denote experimental data. Triangles and diamonds denote simulated data based on the theoretical model for non-free-draining coils with $M = 8.00 \times 10^6$ and 8.12×10^6 g/mol, respectively. The coincidence demonstrates that the theory[26] and the experiment are in complete agreement according to eqs 4 and 8.

already obtained from CONTIN analysis of our experimental data (see Table II at $\theta = 33°$). The deviation of the value of the first characteristic line width Γ_1 was evident with Γ_1 (exp) = 493 s^{-1} and Γ_1 (theory) = 376 s^{-1}. The first peak sat between DK^2 (= 376 s^{-1}) and $DK^2 + 2/\tau_1$ (= 1.4×10^3 s^{-1}), implying that the first peak was a combination of the pure translational term and the first internal term. A larger variance also supported this point. The value of the second characteristic line width Γ_2 was found to be just about the value of $DK^2 + 2/\tau_2$. The results suggested that one could obtain both internal relaxation times of τ_1 and τ_2 only under an ideal condition using data without any noise at $3 \leq x \leq 6$, which was not the real situation. The analysis results from the simulation suggested that both the intensity factor for each term and the separation between the decay rates should be responsible for the CONTIN output. Only Γ_5 could be separated from the other terms when the data contained only a small amount of noise. The simulation confirmed our experimental observations of the second internal relaxation time at this KR_g regime.

Figure 8 shows a comparison of the first cumulant Ω as a function of K. The experimental data (circles) are in complete agreement with the simulated data (triangles from $M_w = 8.00 \times 10^6$ g/mol and diamonds from $M_w = 8.12 \times 10^6$ g/mol) on the basis of the non-free-draining model. The slight deviation in M_w between 8.00×10^6 and 8.12×10^6 g/mol represents uncertainties in the determination of the hydrodynamic radius. This agreement is independent of the method of data analysis.

In conclusion, by means of dynamic light scattering, the first two internal relaxation times, τ_1 and τ_2, could be determined by performing experiments at proper KR_g regimes of $1 \leq x \leq 3$ and $3 \leq x \leq 6$, respectively, for polymer coils at the non-free-draining limit. To our knowledge, it is the first time that the second internal relaxation time has been determined experimentally. The results are in a good agreement with the theoretical predictions by Perico et al.[26] A higher order internal motion term could also be obtained over a higher KR_g regime of $6 < x < 10$, with the deduced relaxation time appearing to coincide with the theoretical relaxation time of the third internal mode. The experimental observation needs further tests using more extended theoretical calculations for a flexible polymer coil in solution in the non-free-draining limit.

Acknowledgment. We gratefully acknowledge support of this project by the Polymer Program, National Science Foundation (Grant No. DMR8921968) and the Department of Energy (Grant No. DEFG0286ER45237A005).

References and Notes

(1) Rouse, P. E., Jr. *J. Chem. Phys.* **1953**, *21*, 1272.
(2) Zimm, B. H. *J. Chem. Phys.* **1956**, *24*, 269.
(3) Chu, B. *Laser Light Scattering*; Academic Press: New York, 1974.
(4) Berne, B. J.; Percora, R. *Dynamic Light Scattering*; Wiley-Interscience: New York, 1976.
(5) Pecora, R. *Dynamic Light Scattering: Applications of Photon Correlation Spectroscopy*; Plenum Press: New York, 1985.
(6) Pecora, R. *J. Chem. Phys.* **1968**, *49*, 1032.
(7) de Gennes, P.-G. *Physics* **1967**, *3*, 37.
(8) Dubois-Violette, E.; de Gennes, P.-G. *Physics* **1967**, *3*, 181.
(9) Chu, B. *J. Polym. Sci.: Polym. Symp.* **1985**, *73*, 137.
(10) Akcasu, A. Z.; Benmouna, M.; Han, C. C. *Polymer* **1980**, *21*, 866.
(11) Koppel, D. E. *J. Chem. Phys.* **1972**, *57*, 4814.
(12) Han, C. C.; Akcasu, A. Z. *Macromolecules* **1981**, *14*, 1080.
(13) King, T. A.; Knox, A.; McAdam, J. D. G. *Chem. Phys. Lett.* **1973**, *19*, 351.
(14) Huang, W.-N. Huang; Frederick, J. E. *Macromolecules* **1974**, *7*, 34.
(15) Tsunashima, Y.; Nemoto, N.; Kurata, M. *Macromolecules* **1983**, *16*, 584.
(16) Nemoto, N.; Makita, Y.; Tsunashima, Y.; Kurata, M. *Macromolecules* **1984**, *17*, 425.
(17) Kim, S. H.; Ramsay, D. J.; Patterson, G. D.; Selser, J. C. *J. Polym. Sci.: Polym. Phys.* **1990**, *28*, 2023.
(18) Sorlie, S. S.; Pecora, R. *Macromolecules* **1988**, *21*, 1437.
(19) Sorlie, S. S.; Pecora, R. *Macromolecules* **1990**, *23*, 487.
(20) Chirico, G.; Baldini, G. *J. Mol. Liq.* **1989**, *41*, 327.
(21) Provencher, S. *Makromol. Chem.* **1979**, *180*, 201.
(22) Ford, J. R.; Chu, B. In *Photon Correlation Techniques in Fluid Mechanics*; Schultz-Dubois, E. O., Ed.; Springer-Verlag: New York, 1983; pp 303–314.
(23) Gulari, E.; Gulari, E.; Tsunashima, Y.; Chu, B. *J. Chem. Phys.* **1979**, *70*, 3965.
(24) Chu, B. *Polym. J.* **1985**, *17*, 225.
(25) Chu, B.; Xu, R.; Maeda, T.; Dhadwal, H. S. *Rev. Sci. Instrum.* **1988**, *59*, 716.
(26) Perico, A.; Piaggio, P.; Cuniberti, C. *J. Chem. Phys.* **1975**, *62*, 2690.
(27) Wang, Z. L.; Chu, B.; Wang, Q.-W.; Fetters, L. In *New Trends in Physics and Physical Chemistry of Polymers*; Lee, L.-H., Ed.; Plenum Publishing Corp.: New York, 1989.
(28) Adam. M.; Delsanti, M. *Macromolecules* **1977**, *10*, 1229.
(29) Zimm, B. H.; Roe, G. M.; Epstein, L. F. *J. Chem. Phys.* **1956**, *24*, 279.
(30) Einaga, Y.; Miyaki, Y.; Fujita, H. *J. Polym. Sci.: Polym. Phys.* **1979**, *17*, 2103.
(31) Nyeo, S.-L.; Chu, B. *Macromolecules* **1989**, *22*, 3998.

Registry No. PS (homopolymer), 9003-53-6; C_6H_6, 71-43-2.